

■ Organic & Supramolecular Chemistry

Novel 1,2,3-Triazole Derivatives as Potential Inhibitors against Covid-19 Main Protease: Synthesis, Characterization, Molecular Docking and DFT Studies

Mohamed Reda Aouad,^{*,[a]} Daoud J. O. Khan,^[a] Musa A. Said,^{*,[a]} Nadia S. Al-Kaff,^[b] Nadjet Rezki,^[a] Adeb A. Ali,^[a] Nahla Bouqellah,^[b] and Mohamed Hagar^[c, d]

The highly contagious nature of Covid-19 attracted us to this challenging area of research, mainly because the disease is spreading very fast and until now, no effective method of a safe treatment or a vaccine is developed. A library of novel 1,2,3-triazoles based 1,2,4-triazole, 1,3,4-oxadiazole and/or 1,3,4-thiadiazole scaffolds were designed and successfully synthesized. Different spectroscopic tools efficiently characterized all the newly synthesized hybrid molecules. An interesting finding is that some of the newly designed compounds revealed two isomeric forms. The ratio is affected by the size of the attached group as well as the type of the heteroatom forming the side ring attached to the central 1,2,3-triazole ring. The experimental spectroscopic data is in agreement with the DFT calculations at B3LYP 6-31G (d,p) with regard to the

geometrical conformation of the prepared compounds. The DFT results revealed that the stability of one isomeric form over the other in the range of 0.057–0.161 Kcal mol⁻¹. A docking study was performed using PyRx and AutoDockVina to investigate the activity of the prepared 1,2,3-triazoles as antiviral agents. Bond affinity scores of the 1,2,3-triazole derivatives were detected in the range of –6.0 to –8.8 kcal/mol showing binding to the active sites of the 6LU7 protease and hence could be anticipated to inhibit the activity of the enzyme. Verification of the docking results was performed using the M^{Pro} alignment of coronaviruses substrate-binding pockets of COVID-19 against the ligands. As per these results, it can be proposed that the title hybrid molecules are acceptable candidates against COVID-19 for possible medicinal agents.

1. Introduction

The current health and economic concerns of the entire world due to Covid-19, motivated many research groups to dig for safe and effective treatment or/and vaccine for this fast-spreading epidemic.^[1–14] The eruption of this novel COVID-19 or 2019-CoV infection has posed a substantial challenge to the international scientific research community after the World Health Organization could not rule out the airborne transmission of coronavirus.^[15] It is well known that there are no effective and non-toxic specific antiviral treatments or vaccines for this disease so far. Therefore, governments have to depend, mainly, on applying severe preventive and control measures

that reduce the risk of possible disease spread, however, this solved a problem and created another.^[16] Hence, in the absence of a cure for this virus, the door became widely open for urgent alternative approaches to control the spread of the disease. It has been confirmed that this virus is covered through folded structure and has a single-stranded RNA genome.^[5] Possible easy and useful backbone approaches for many researchers, to help to face this international challenge, are the investigation of the fascinating pharmacophore and computational approaches.^[17] Because the computational approach is a low cost, less time consumption and less error to identify promising drugs, hence, we have been motivated to address this challenge to explore the nitrogen heterocyclic compounds as potent antiviral candidates. It is related, here, to note that the first protein-ligand docking method was published more than three decades ago.^[18] Heterocyclic containing nitrogen atoms have shown effective antiviral activities. For example, Ribavirin and Taribavirin namely 1-((2*R*,3*R*,4*S*,5*R*)-3,4-dihydroxy-5-(hydroxymethyl)tetrahydrofuran-2-yl)-1*H*-1,2,4-triazole-3-carboxamide and 1-*D*-ribofuranosyl-1,2,4-triazole-3-carboxamide, are well known as nucleosides based 1,2,4-triazole motif and are the most effective antiviral drugs broadly approved. They have been systematically used against herpes simplex virus (HSV), human immunodeficiency virus (HIV-1), respiratory syncytial, influenza virus and hepatitis C virus.^[19] However, due to their broad cytotoxicity, their routine clinical uses became limited, therefore, recent efforts have been reported to modify the standard core by replacing the 1,2,4-triazole motif with

[a] Prof. M. R. Aouad, D. J. O. Khan, Dr. M. A. Said, Prof. N. Rezki, Dr. A. A. Ali
Department of Chemistry, College of Science, Taibah University, Al-Madinah Al-Munawarah 30002, Saudi Arabia
E-mail: maouad@taibahu.edu.sa
mr_aouad@yahoo.fr
masaid@taibahu.edu.sa

[b] Dr. N. S. Al-Kaff, Dr. N. Bouqellah
Department of Biology, College of Science, Taibah University, Al-Madinah Al-Munawarah 30002, Saudi Arabia

[c] Dr. M. Hagar
Department of Chemistry, College of Sciences, Yanbu, Taibah University, Yanbu, 30799, Saudi Arabia

[d] Dr. M. Hagar
Department of Chemistry, Faculty of Science, Alexandria University, Alexandria 21321, Egypt

Supporting information for this article is available on the WWW under <https://doi.org/10.1002/slct.202100522>

another nitrogen heterocyclic ring to develop some novel ribavirin analogs. For example, new 1,2,3-triazoles based ribavirin analogs have been investigated,^[20] (Figure 1), which were proved to be more effective than ribavirin in terms of antiviral activity.

Besides, 1,3,4-oxadiazole and 1,3,4-thiadiazole frameworks have already been reported for their antiviral properties. Many antiviral drugs were documented to append the thiadiazole^[21–23] oxadiazole^[24] and/or 1,2,4-triazole core^[25–27] in their structures, (Figure 2).

Anticipation for various other ribavirin analogs has led us to investigate more structural modifications of it to evaluate their pro-antiviral drug results compared to ribavirin. Moreover, triazole core provides diverse pharmacophoric properties and their hybrid with other conjugates, and their related compounds are used as leads in medicinal chemistry.^[27–30] An interesting addition is that 1,3,4-oxadiazole core can exhibit supramolecular assembly through N–H...S and C–H...S, point-to-face C–H... π contacts and π ... π stacking interactions.^[31] Based on these findings, it is very promising that the present research will stimulate endeavors in the design and development of newer patent antiviral candidates. For this, the 1,2,3-triazoles based functionalized 1,2,4-triazole, 1,3,4-thiadiazole and/or 1,3,4-oxadiazole core have been successfully synthesized and fully characterized using various spectroscopic techniques. Besides, the spectroscopic data of the isomeric forms were compared with the DFT results in this study. In this research study, one main protease crystallized COVID-19

structure (PDB ID: 6LU7) has been chosen for molecular modeling against our novel compounds. Computational docking analysis was performed using PyRx, AutoDockVina option based on scoring functions.^[32] The outcomes exhibited multi-hydrogen bonding and hydrophobic interactions between the 1,2,3-triazole derivatives with 6LU7 protease. Docking bond affinity, (kcal/mol), scores of 1,2,3-triazole derivatives were detected between –6.0 and –8.8 kcal/mol. As per these results, it can be proposed that our 1,2,3-triazole derivatives are good candidates against COVID-19 for possible medicinal agent.

2. Results and discussion

2.1. Chemistry

A series of novel 1,2,3-triazoles tethered bis-1,2,4-triazole, bis-1,3,4-oxadiazole and/or bis-1,3,4-thiadiazole motif were synthesized from the newly designed 1,2,3-triazole diester $\mathbf{3}$ as a starting material (Schemes 1–3). The approach adopted for the synthesis of dimethyl 1-(4-bromophenyl)-1*H*-1,2,3-triazole-4,5-dicarboxylate ($\mathbf{3}$) was based on a free solvent 1,3-dipolar cycloaddition reaction of the dimethylacetylenedicarboxylate $\mathbf{1}$ with *p*-bromoazidobenzene $\mathbf{2}$ at 80–90 °C for only 3 min (Scheme 1). The used aryl azide was prepared *via* the diazotization of *p*-bromoaniline in the presence of sodium nitrite solution in acidic media, followed by the azidolysis with sodium azide as described before.^[33]

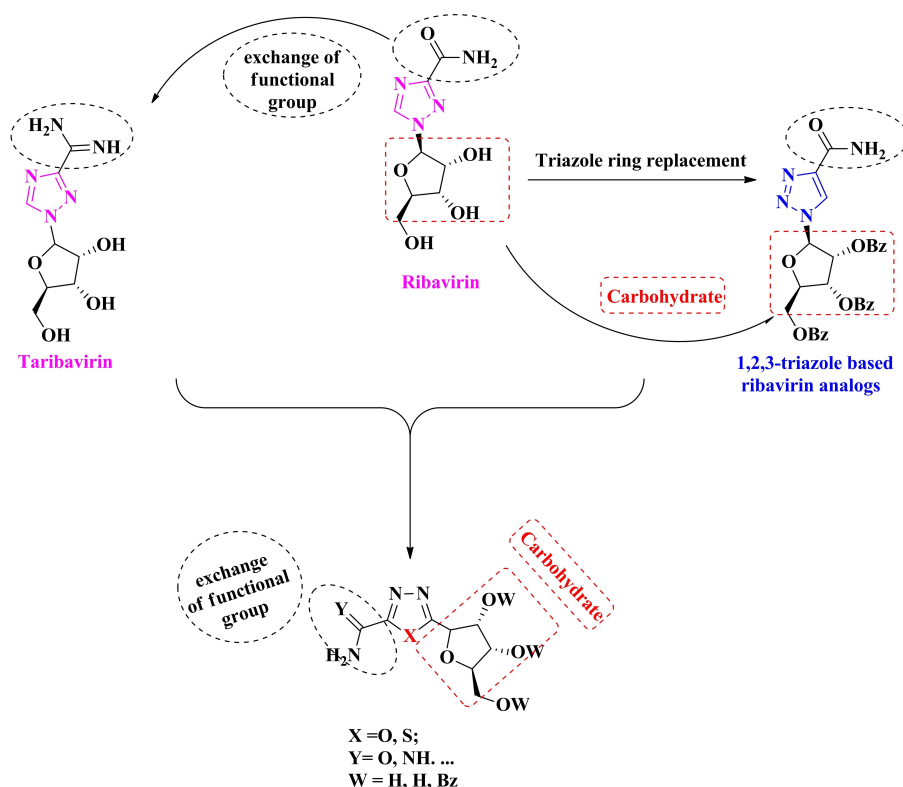


Figure 1. Coherent proposal for designing ribavirin-based nucleoside analogs.

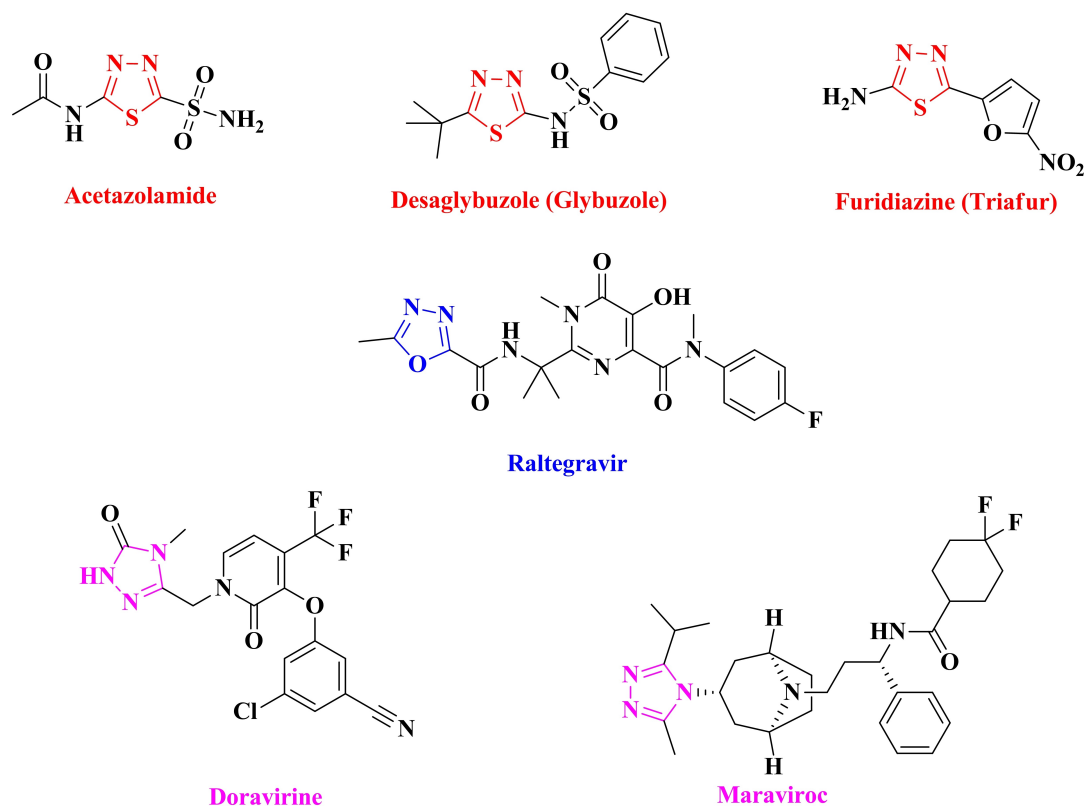
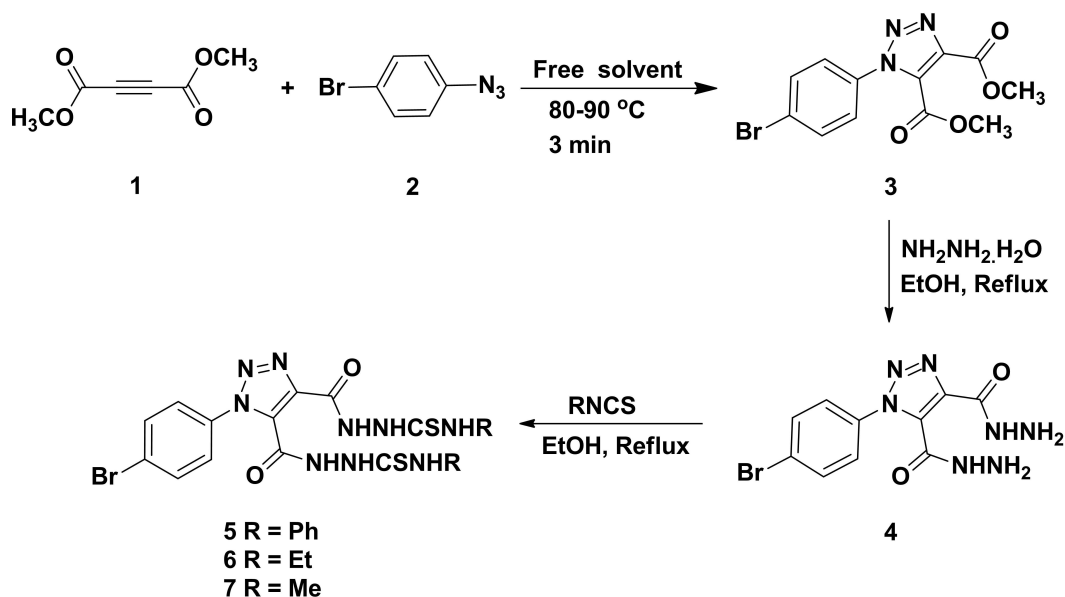


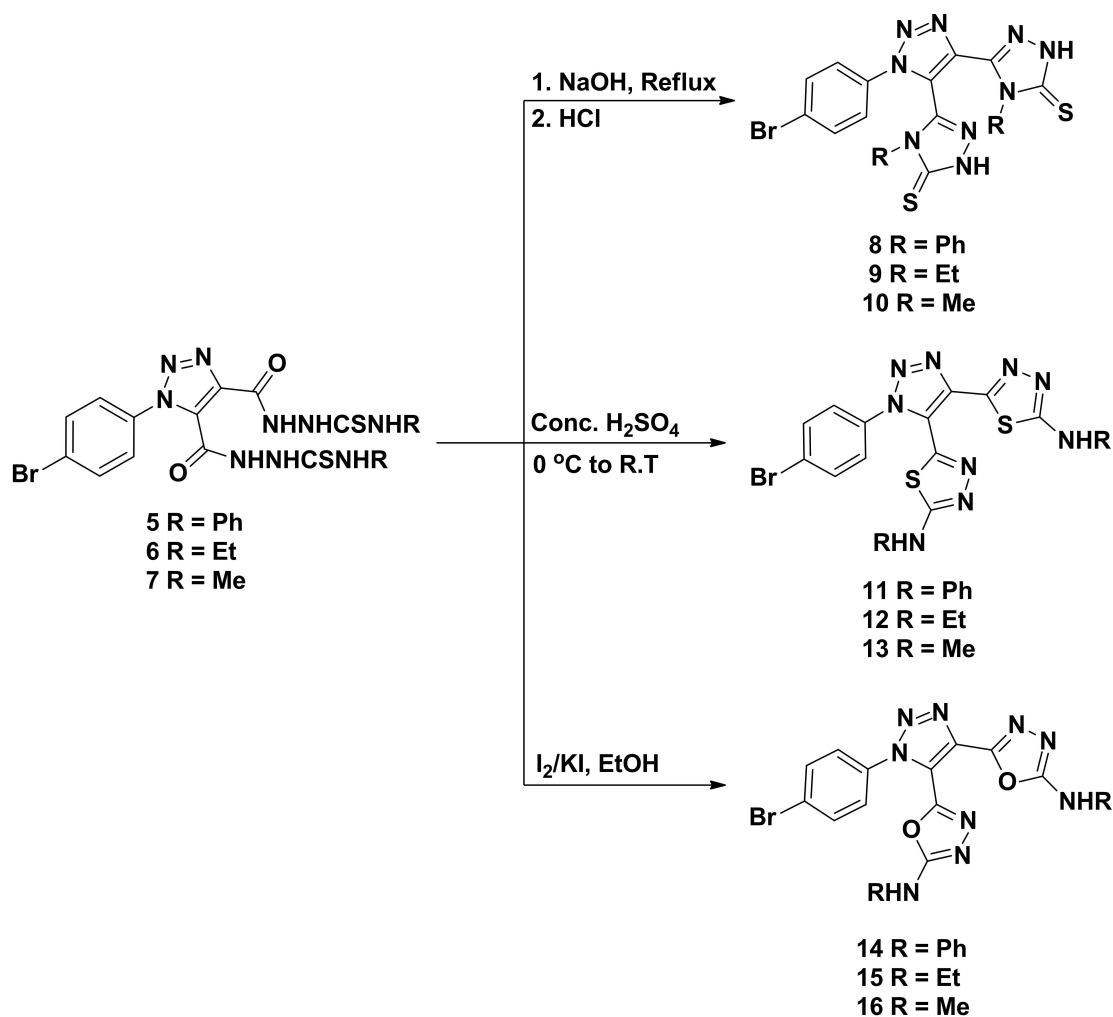
Figure 2. Structure of antiviral drugs containing 1,3,4-thiadiazole, 1,3,4-oxadiazole and/or 1,2,4-triazole.



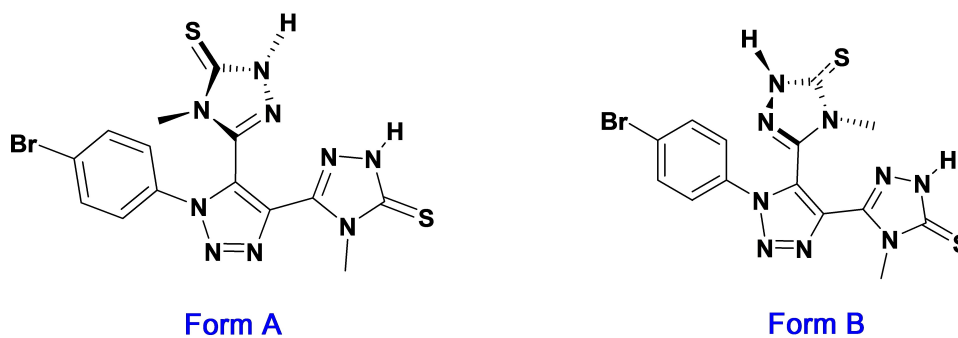
Scheme 1. Synthesis of 1,2,3-triazoles 3–7 bearing different functionalities.

The success of such 1,3-dipolar cycloaddition was supported by the spectroscopic results of the resulted 1,2,3-triazole-bis-esters **3** which were in agreement with its proposed structure. The $^1\text{H-NMR}$ spectrum displayed two distinguishable singlets at 3.88 and 3.94 ppm of the two nonequivalent

methoxy groups of the ester functionalities. The two doublets recorded at 7.64 and 7.87 ppm were attributed to the protons of the *p*-benzene residue. Additionally, the $^{13}\text{C-NMR}$ spectrum revealed no signals on the *sp*-carbon regions confirming their involvement in the cycloaddition reaction, and two additional



Scheme 2. Synthesis of 1,2,3-triazoles clubbing bis-1,2,4-triazole 8–10, bis-1,3,4-thiadiazole 11–13 and/or bis-1,3,4-oxadiazole 14–16.



Scheme 3. Proposed conformational isomers for bis-1,2,3-triazoles 10.

signals appeared at 158.50 and 159.79 ppm characteristic for the two nonequivalent carbonyls (C=O) ester carbons. The two-methyl ester carbons (CH₃) resonated separately in the aliphatic region at 52.77 and 54.00 ppm.

The hydrazinolysis of the resulted 1,2,3-triazole-based ester 3 was carried out through its thermal treatment with hydrazine hydrate in refluxing ethanol for 4 hr and has successfully

proceeded to afford the corresponding bis-acid hydrazide(4) in 90% yield, (Scheme 1). The structure of the acid hydrazide 4 was deduced based on its NMR spectral data. The ¹H-NMR revealed the disappearance of the two methoxy groups and the appearance of two new broad singlets at 4.70 and 10.95 ppm attributed to NH₂ and NH groups, respectively, confirming the success of hydrazinolysis reaction. The ¹³C-NMR

spectrum revealed the absence of the two methoxy carbons as well as the upfield shifting of the two carbonyls from the ester moieties (158.50 and 159.79 ppm) to the amide moieties (155.45 and 158.50 ppm).

The reaction between isothiocyanates and active N-H groups resembles the early known proposed procedure by Douglas and Dains,^[34] however, this methodology has been recently updated for related thiourea-related compounds.^[35] Three novel bis-acid thiosemicarbazide carrying 1,2,3-triazole scaffold 5–7 were successfully prepared in 88–89% yields by refluxing an ethanolic solution of the bis-acid hydrazide 4 with phenyl, ethyl and/or methylisothiocyanate for 6 hr, (Scheme 1). Structural elucidation of the new acid thiosemicarbazides 5–7 was carried out based on their IR, ¹H, ¹³C-NMR and elemental analysis data. Thus, the ¹H-NMR spectrum of the *N*-ethyl thiosemicarbazide derivative 6 revealed two sets of triplets on the alkyl group region at 1.06 and 1.12 and a multiplet at 3.47 ppm related to the two unsymmetrical ethyl groups. The two broad singlets recorded at 8.00 and 8.14 ppm were attributed to the two non-equivalents NH protons. Moreover, four singlets appeared at 9.54, 9.56, 11.11 and 11.14 ppm integrated for four protons related to the amidic (CONH) and thioamidic (CSNH) protons, respectively. The aromatic protons were also observed in their respective chemical shifts (7.64 and 7.85 ppm). Its ¹³C-NMR data also supported the structure by the appearance of new aliphatic carbons around 14.30–39.46 ppm belonging to the two ethyl groups. Also, new carbon signals were recorded at 189.77 and 191.46 ppm confirming the presence of the thiocarbonyl carbons (C=S).

The targeted 1,2,3-triazole-*bis*(1,2,4-triazole-3-thione) 8–10 were easily obtained *via* base-assisted thermal intramolecular cyclization of their acid thiosemicarbazide precursors 5–7 in refluxing aqueous solution of sodium hydroxide (10% NaOH), (Scheme 2).

The structures of the obtained 1,2,4-triazoles were elucidated based on their spectroscopic analysis. The ¹H-NMR spectra of the three triazoles 8–10 showed clearly the disappearance of the amidic and the thioamidic protons of the starting material which confirmed their involvement in the intramolecular cyclization furnishing on the formation of the 1,2,4-triazole moieties. The spectra also revealed the presence of four distinct singlets around 9.12–14.69 ppm integrated for two protons, belonging to the two triazole NH protons. However, we have deduced that 1,2,4-triazoles 8–10 existed as a mixture of two conformational isomers A and B with different ratios. As an example, the ¹H-NMR spectrum of compound 10 was discussed, (Figure 3). The singlets recorded at 9.52 and 14.10 ppm are associated with the NH protons of the conformer A (75%). In the case of conformer B, singlets for NH protons were observed at 14.13, and 14.37 ppm, respectively (25%). Consequently, it could be concluded that both 1,2,4-triazoles rings were formed in thione form only for the two conformational isomers (Scheme 3).

Moreover, the ¹³C-NMR spectrum (Figure 4) exhibited clearly the disappearance of the thiosemicarbazide carbonyl carbons (C=O) and the appearance of (C=S) signals at 168.39, 168.77, 168.78 ppm confirming the predominance of the thione isomers. These results were in agreement with that previously

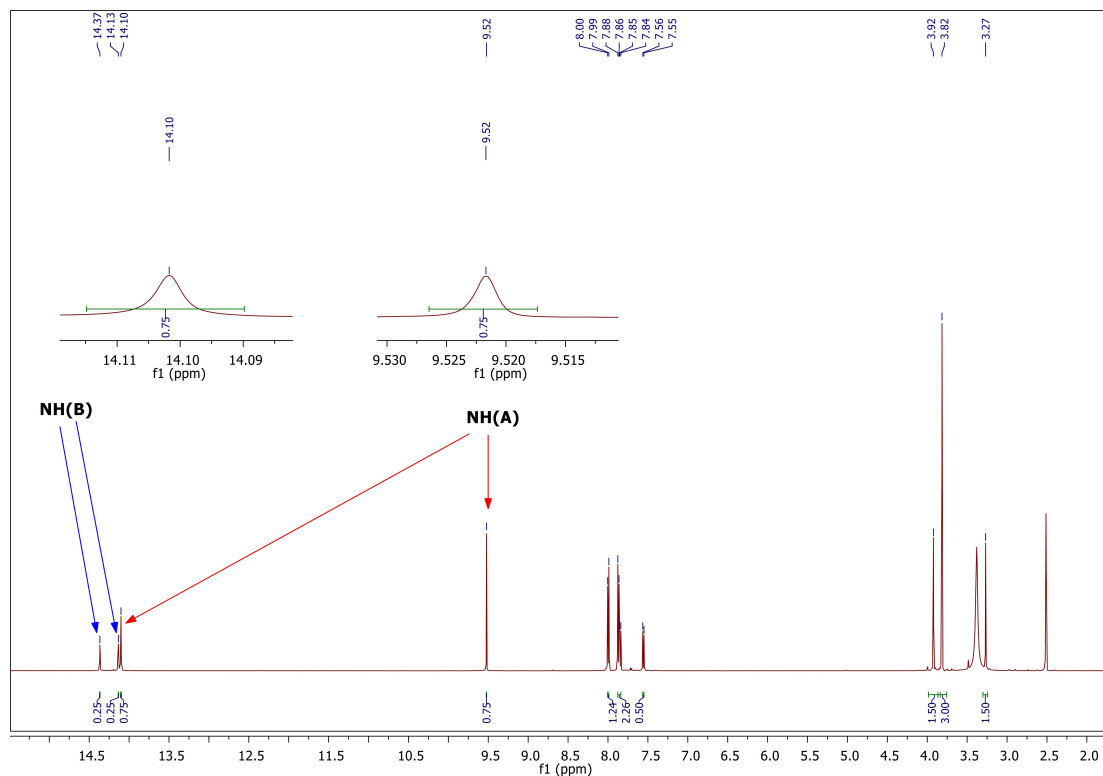


Figure 3. ¹H-NMR spectrum of compound 10.

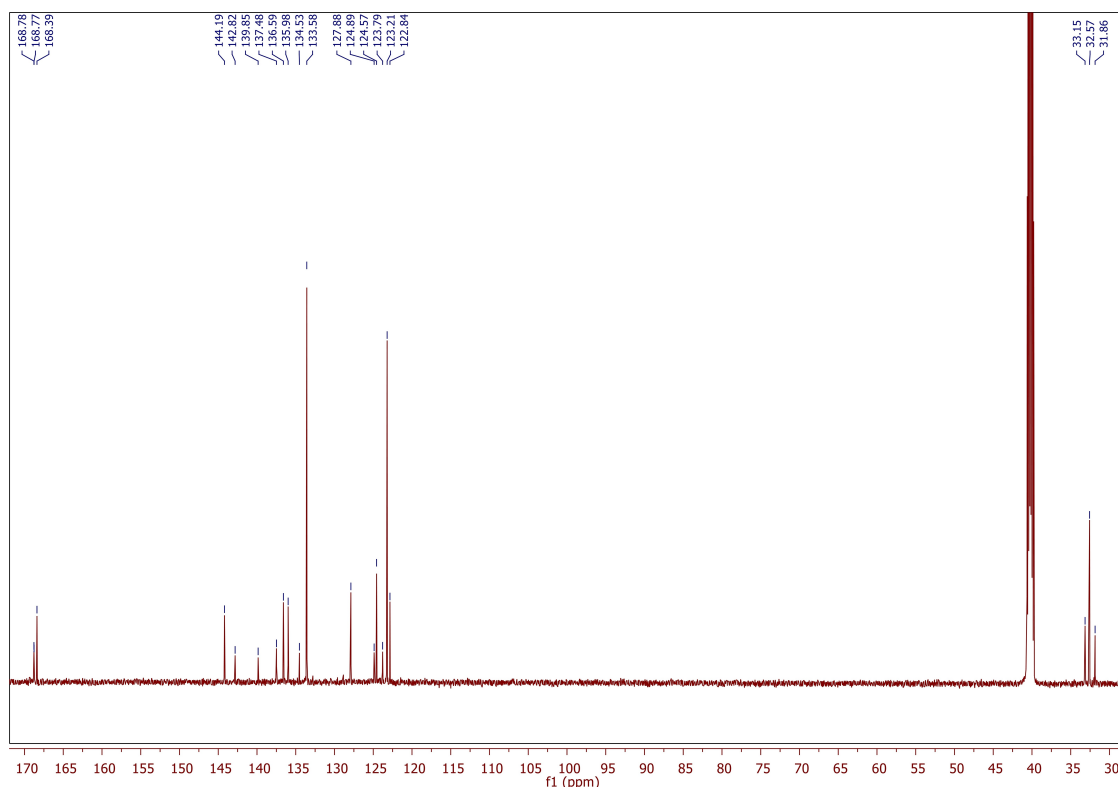


Figure 4. ^{13}C -NMR spectrum of compound 10.

reported where only the thione tautomer has been isolated.^[36–38]

The IR spectra of triazoles **8–10** revealed the common triazole characteristic absorption peaks at $1295\text{--}1310\text{ cm}^{-1}$ and $1620\text{--}1630\text{ cm}^{-1}$ attributed to (C=S) and (C=N), respectively. Besides, the spectra showed also the presence of absorption bands at $3220\text{--}3365\text{ cm}^{-1}$ assigned to NH groups, which confirmed the formation of the triazole rings in the thione form. These results were in agreement with those reported previously for similar compounds.^[39,40]

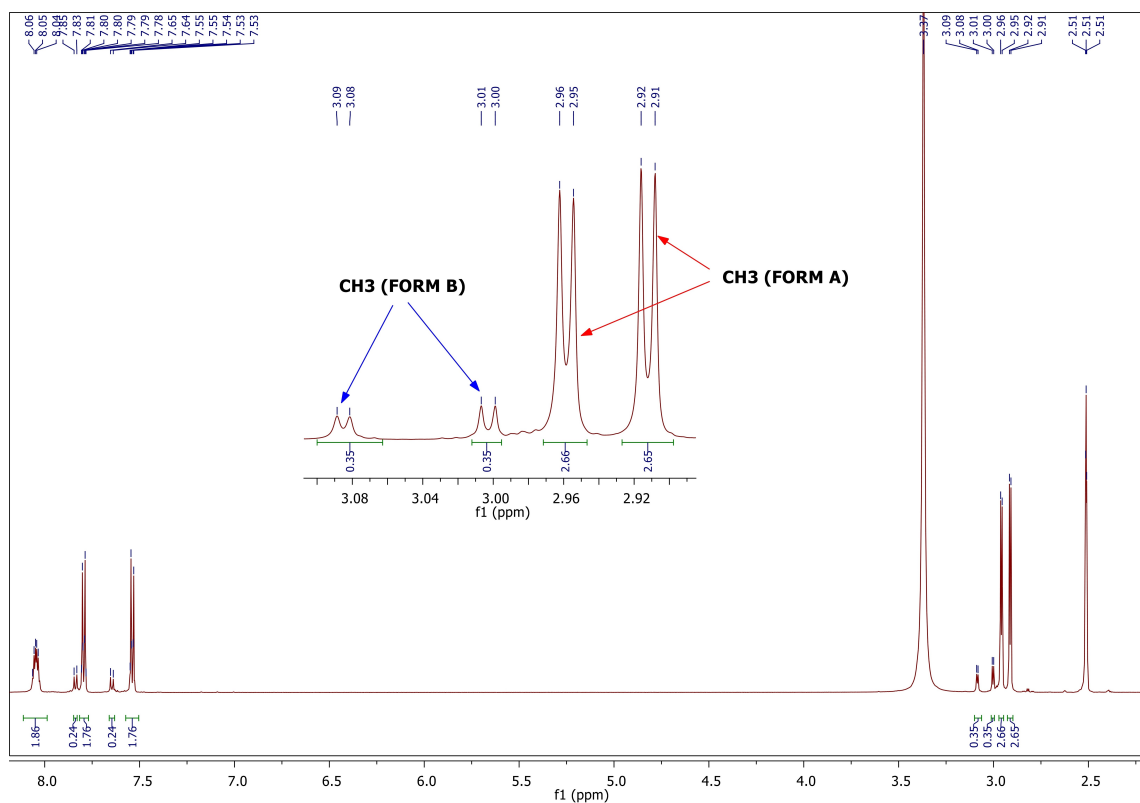
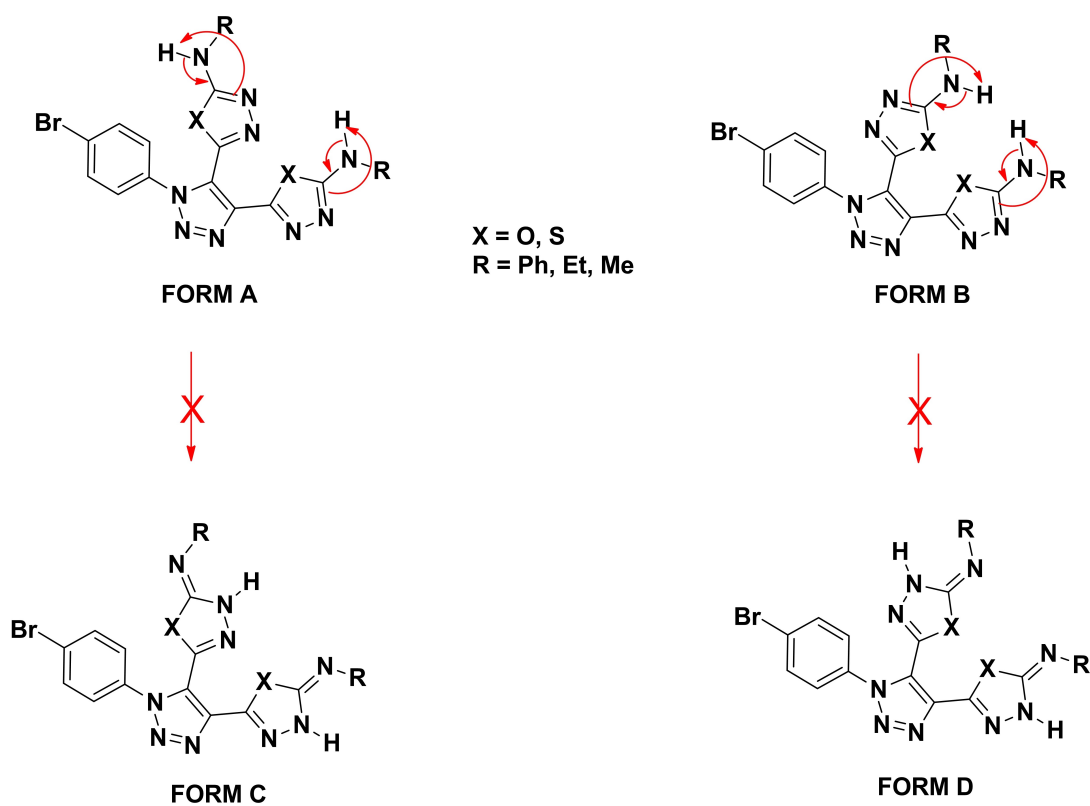
The same acid thiosemicarbazides **5–7** also experienced dehydrative intramolecular cyclization reaction, in the presence of concentrated sulfuric acid at 0°C proceeded to give the corresponding bis-(2-aryl/alkylamino-1,3,4-thiadiazoles) derivatives appending 1,2,3-triazole core **11–13** in good yields (80–82%). On the other hand, the acid thiosemicarbazide intermediates **5–7** were also oxidatively cyclized in the presence of I_2/KI solution in ethanol yielding 77–80% yields of the targeted 1,2,3-triazole-bis-(2-aryl/alkylamino-1,3,4-oxadiazoles) **14–16** (Scheme 2). To confirm the formation of the 1,3,4-thiadiazoles **11–13** and the 1,3,4-oxadiazoles **14–16**, the spectral data of compound **13** were discussed. Thus, the ^1H NMR spectrum of the *N*-methylamino thiadiazole derivative **13**, (Figure 5) did not show the NH-protons of its acid thiosemicarbazide precursor **7** and the appearance of the two diagnostic exocyclic thiadiazole NH-protons as a multiplet at 8.03–8.06 ppm. The aliphatic region showed two distinct doublets at 2.92 and 2.96 ppm related to the two unsymmetrical CH_3NH protons (88%). Addi-

tionally, two minor doublets were displayed at 3.01 and 3.09 ppm assignable to the same CH_3NH protons (12%).

Consequently, it could be concluded that the presence of these two sets of doublets supports the formation of two conformational isomers A and B of the tautomeric amine form. Besides, the absence of diagnostic singlets characteristic for the isolated methyl groups eliminated the possibility of formation of the tautomeric imine C and D forms. The same pattern was observed for aromatic protons (Scheme 4).

In addition, the ^{13}C NMR analysis approved the formation of the expected thiadiazole **13** (Figure 6) through the absence of the carbonyl and thiocarbonyl carbons (C=O and C=S) of its corresponding starting material, which confirmed their involvement in the intramolecular cyclization. The aliphatic region in the ^{13}C -NMR spectrum also supported the presence of two conformational isomers, where four signals assigned to the methyl groups were recorded. Two methyl groups appeared at 31.69 and 31.77 ppm (for the major isomer), and at 31.56 and 31.91 ppm for the minor one, (Figure 6).

The formation of the thiadiazoles **11–13** and oxadiazoles **14–16** was also deduced based on their IR spectral data, which showed the disappearance of the carbonyl (C=O) and thiocarbonyl (C=S) groups in their IR spectra and the appearance of characteristic absorption bands near $1620\text{--}1635$ and $3225\text{--}3340\text{ cm}^{-1}$ attributed to the C=N and NH groups, respectively. The IR spectral data were in accordance with that previously reported for related compounds.^[39,40]

Figure 5. $^1\text{H-NMR}$ spectrum of compound 13.

Scheme 4. Proposed conformational isomers for bis-1,3,4-thiadiazole 11–13 and bis-1,3,4-oxadiazole 14–16.

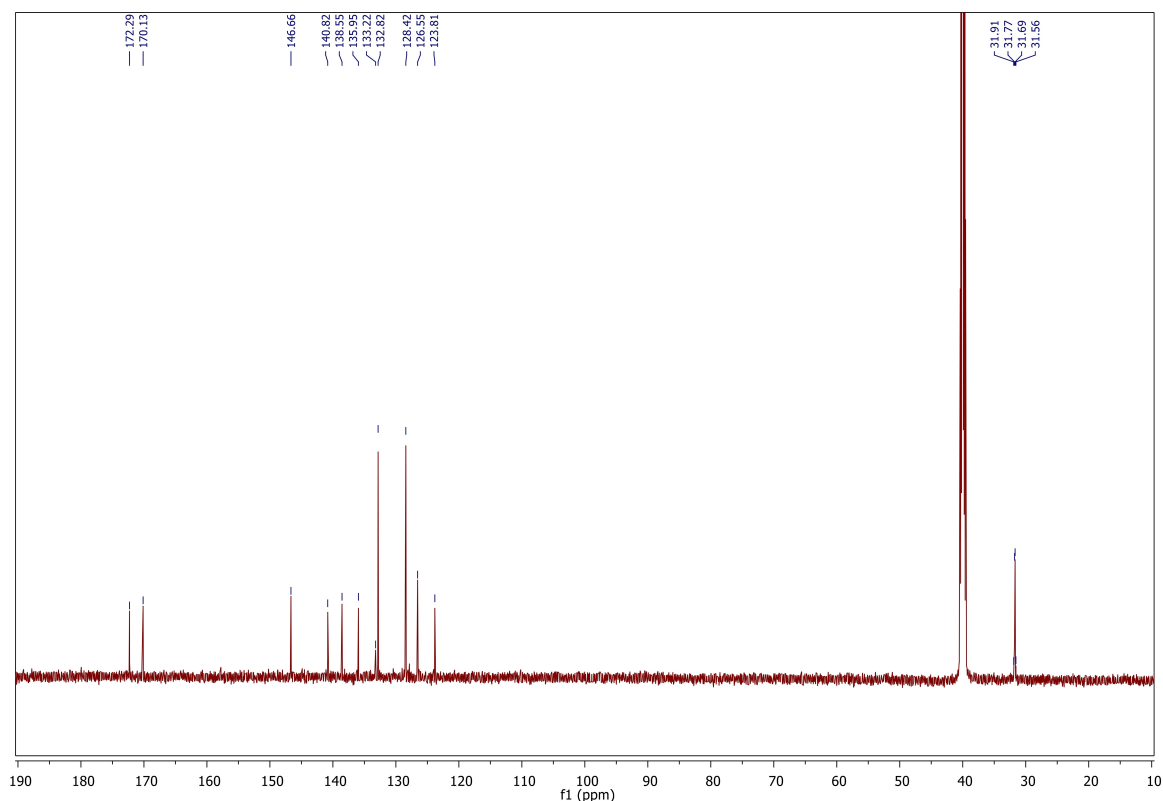


Figure 6. ^{13}C -NMR spectrum of compound 13.

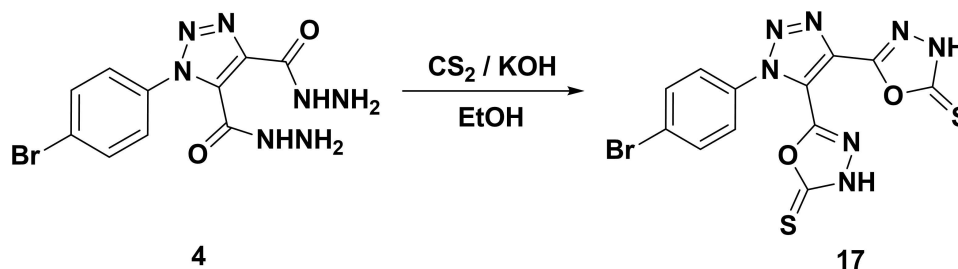
On the other hand, the bis-(1,3,4-oxadiazole-2-thione), **17** was also designed and synthesized from 1,2,3-triazole bearing bis-acid hydrazide **4**. Thus, thermal treatment of compound **4** with carbon disulfide in ethanolic potassium hydroxide solution yielded the desired bis-1,3,4-oxadiazole-2-thione **17** in 80% yield (Scheme 5).

The formation of oxadiazole **17** was confirmed by its spectral data analyses. The ^1H -NMR spectrum revealed clearly the disappearance of amine and amide protons of the acid hydrazide linkage, and the appearance of two new broad singlets at 12.16 and 15.11 ppm assigned to the unsymmetrical NH protons of the oxadiazole rings confirming the predominance of the thione form. The aromatic protons appeared as two doublets at 7.73 and 7.89 ppm. Besides, the ^{13}C -NMR spectrum clearly confirmed the formation of the two oxadia-

zole rings in their thione form through the appearance of two nonequivalent C=S peaks at 178.02 and 178.10 ppm. The structure of the synthesized oxadiazole **17** was also confirmed by its IR spectrum which clearly showed two characteristic bands around $3295\text{--}3350\text{ cm}^{-1}$ and 1290 cm^{-1} assigned to NH and C=S groups, respectively.

2.2. DFT molecular structure

The presence of isomeric forms for compounds **8**, **10** and **13** motivated us to do further structural study by DFT method at B3LYP 6-311G (d,p) for a complete understanding of the geometrical conformation preferences of the prepared compounds. In fact, various conformations are likely depending on the mutual orientations of the thiadiazole groups with respect



Scheme 5. Synthesis of 1,2,3-triazole bearing bis-(1,3,4-oxadiazole-2-thione) **17**.

to the triazole ring.^[31] Experimentally, the size of the attached substituents plays an important role to favor the predominance of one conformer over the other form. This is due to the degree of steric hindrance of the attached group on aromatic rings. The DFT calculations were carried out for a single molecule in a gas phase for the proposed conformers of the methyl and the phenyl derivatives to illustrate the effect of the size of the attached group in 1,2,3-triazole derivatives in this study.

To investigate the optimized structure, we have considered the rotation of C5–C6 bond of the perpendicular triazole ring with respect to the other rings plane, which results in the change in dihedral N1–C5–C6–N7. It is clear that, the investigated compounds have several expected conformations depending on the mutual orientations of the connected rings similar to analogous reported thiadiazoles. However, the reported thiazolo derivatives are less crowded than our investigated compounds. Different conformations of the reported thiadiazoles rose due to the mutual orientations of the thiadiazolyle and 2-hydroxyl groups with respect to the pyrrolidine ring. Three conformers have been studied and the conformational analysis was conducted to reveal the energy difference was in the range of 21.9 kJ/mol^[41] The structure

deviates of our investigated compounds from planarity due to steric hindrance created by the triazole rings as well as the attached methyl groups. Therefore, the scanned potential energy surface (PES) along dihedral N1–C5–C6–N7 was carried out and the scan curve was shown in Figure 7. The PES scan curve could show the optimized geometrical structure of the corresponding global minima. It is obvious that there is an existence of two energetically least lying conformers A and B.

The optimized geometrical structures of the methyl and the phenyl derivatives are shown in Figure 8. The detailed calculations were performed for the two most stable conformational isomers of compounds 8 and 10. This involved performing a geometry optimization on each isomer to determine the minimum energy structure, followed by a frequency calculation at the optimized geometry during which various thermochemical quantities are also computed.

In principle, several conformations are expected depending on the mutual orientations of the connected rings. In order to find out the relative stability of each isomeric conformer for the phenyl and methyl derivatives, the corrected energy and the thermodynamic properties (enthalpy (H), and free energy (G)) were computed, Table 1.

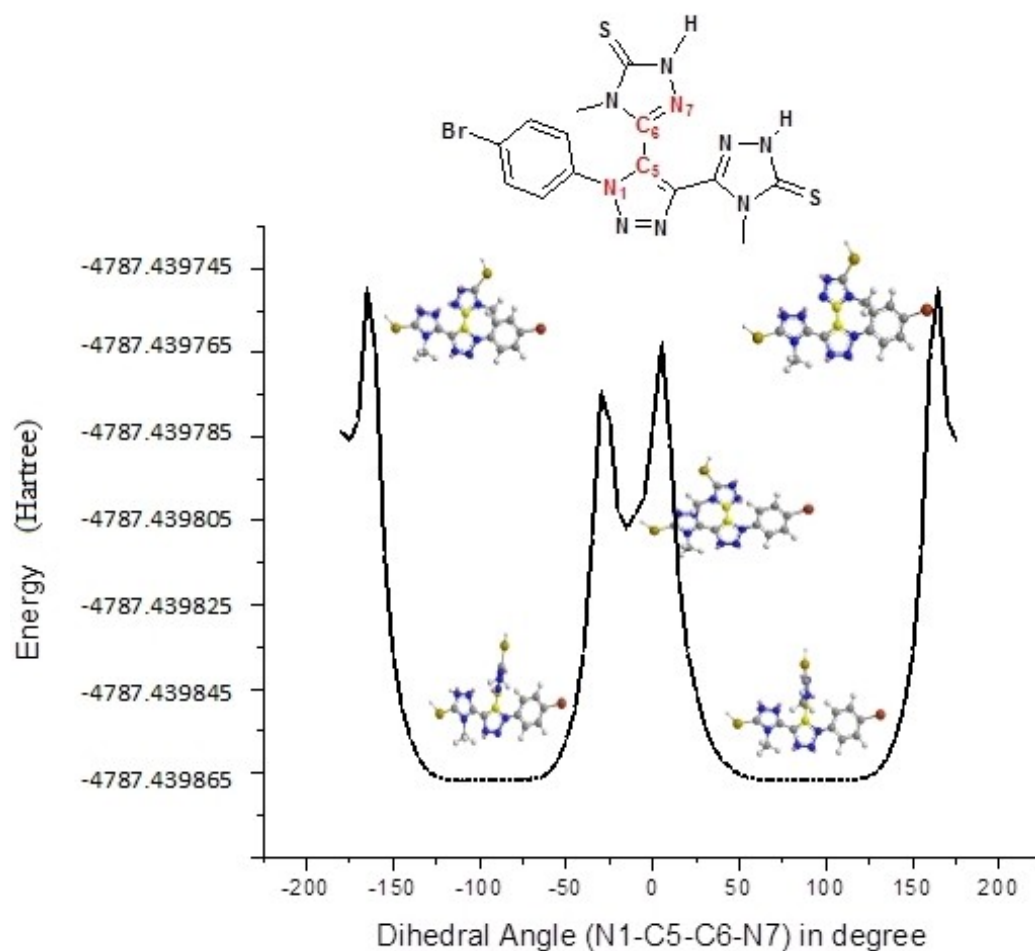


Figure 7. Calculated potential function for internal rotation along N1–C5–C6–N7 dihedral angle for the methyl derivative 10.

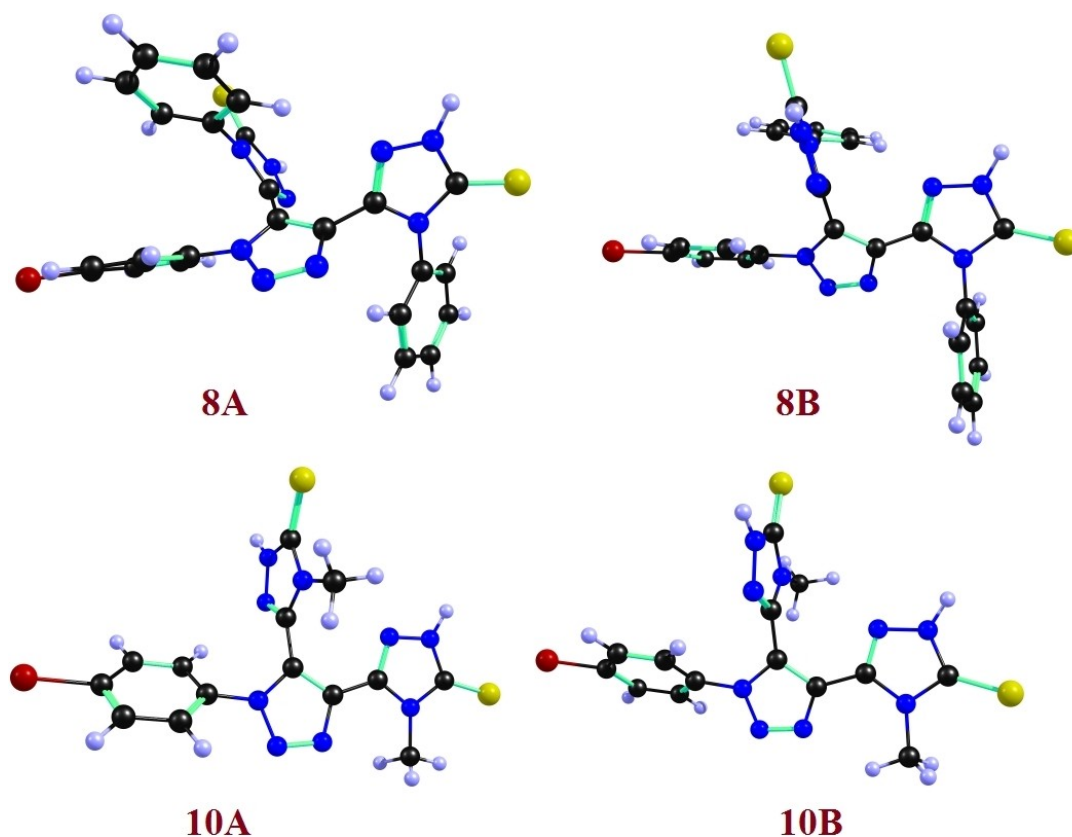


Figure 8. Optimized molecular structure of studied conformers A and B of compounds 8 and 10.

Table 1. B3LYP calculated thermal-corrected energy, thermodynamic properties: enthalpy (H), free energy (G), ΔE , ΔH , ΔG values for isomeric forms of compounds 8, 10 and 13 using 6-311G (d,p) basis set.										
Parameters	ΔG (kcal/mol)	ΔH (kcal/mol)	ΔE (kcal/mol)	G (hartrees)	H (hartrees)	E_{corr} (hartrees)	E_{tot} (hartrees)	ZPVE (hartrees)	Form	Comp.
0	0	0	0	-4404.052881	-4403.970334	-4403.971279	-4403.994792	0.269540	A	8
0.023199	0.023826	0.057057	-4404.052502	-4403.970297	-4403.971241	-4403.994701	0.269707	B		
0.036366	0.036366	0.06897	-4787.507199	-4787.409144	-4787.410088	-4787.439745	0.373745	A	10	
0	0	0	-4787.508066	-4787.409202	-4787.410146	-4787.439855	0.373618	B		
0.030723	0.030723	0.160512	-4404.001120	-4403.916568	-4403.917512	-4403.941925	0.264644	A	13	
0	0	0	-4404.001166	-4403.916749	-4403.917693	-4403.942025	0.264645	B		

The results of the DFT calculations revealed that form A for compound 8 is in a lower energy structure than the other form B by 0.057 Kcal/mol, hence more stable than its conformational isomer. However, form B is more stable than the other form A for compound 10. The energy difference was by 0.069 Kcal/mol. The slightly higher energy between both conformers A and B of compound 8 could be illustrated in terms of the steric hindrance of the bulk phenyl group with respect to the small methyl group of compound 10. Furthermore, the stability pattern is reversed by changing the attached group; conformer B is more stable for compound 8 while conformer A is more stable for compound 10. Further, the small difference in energy between both conformers of either the methyl or the phenyl derivatives does not mean their presence of interconverting

equilibrium. This is because the presence of both 1,2,3-triazole rings adjacent to each other prohibits the free rotation around the C–C single bond. Such difference in energy could be explained in terms of the kinetic and thermodynamic stabilities of form B of compound 8 and A for compound 10.

The effect of the type of the heteroatom of the attached ring on the central 1,2,3-triazole group was also investigated by stimulation the molecular geometry of both conformers A and B for their methyl derivatives of compound 13. As shown in Table 1, the thiadiazole derivative 13 goes in a similar trend as for compound 10. Conformer A is less stable than B by 0.161 Kcal/mol. The difference in stability of one conformer with respect to the other due to different heterocycles could be illustrated in terms of the degree of conjugation that could

give a certain conformer more stability than the other (Figure 9).

2.3. Docking studies

The purpose of this docking study, at this critical time, is to examine how 1,2,3-triazole based ligands might approach the active site of the main protease for Covid-19, (M^{pro} , PDB 6LU7) towards finding antiviral agents for this damaging disease. The docked molecules, fitted in a cavity held by hydrogen bonding and hydrophobic interaction with the active sites of protease 6LU7 are presented in Table 2. The binding affinities to the biological targets are usually considered in choosing possible drug candidates. Docking scores were considered the binding affinities (kcal/mol) with more negative values indicating better binding strength.

Several coronaviruses (HCoVs) infect humans were identified and divided into two groups depending upon symptoms causes; the first group causes mild upper respiratory diseases namely, HCoV-OC43, HCoV-NL63, HCoV-HKU, and HCoV-229E. The second group causes severe acute lower respiratory syndrome namely coronavirus (SARS-CoV), Middle East respiratory syndrome coronavirus (MERS-CoV) and the newly emerged coronavirus, COVID-19.^[42] The phylogenetic tree divided these groups of coronaviruses into three clusters based on the similarity on their amino sequence of M^{pro} , Figure 9. The first cluster contains HCoV-229E, HCoV-NL63 and MERS-CoV, the second cluster contains COVID-19 and SARS-CoV and finally, the third cluster contains HCoV-HKU1 and HCoV-OC43. Based on Jin and others in 2020, the total number of amino acids in COVID-19 M^{pro} is 306.^[43] Promoters of coronaviruses are composed of three domains; domain I, contains amino acids from 8 to 101, domain II, which starts from 102 to 184 and III, from 201 to 303 residues. A long loop region covered by residues 185–200 which is the region between domains II and III and Figure 10, I. Conserved residues in the coronaviruses are distributed in different substrate binding sites, P1, P2, P4 and P5. Substrate-binding was identified in a cleft between domain I and II.^[43] COVID-19 binding pocket was comparable to that found in other coronaviruses.^[44–48]

All 1,2,3-triazoles were docked to substrate-binding site residues of COVID-19. 22 amino acids are structuring the substrate-binding site, 50% of them are conserved among the coronaviruses aligned Figure 10. The closest coronavirus to COVID-19 is SARS-CoV, however, there is one amino acid (S46) in the substrate-binding site which is not alike. Nevertheless, none of the 1,2,3-triazoles tested bounded to this amino acid (S46) in COVID-19. Six identical amino acids were identified between COVID-19 and MERS-CoV. They are S45, M49, H 164, P168, T190 and A191. Yet, there are many amino acid residues in the pockets of COVID-19 and MERS-CoV is not alike.

The box plot was created for the variation with 1,2,3-triazole derivatives in their binding affinity to amino acid residues of COVID-19, Figure 11.

Docking results of 1,2,3-triazole derivatives detected in this study found to have the highest H-bonding and hydrophobic interactions were with E166; ligands 12 and 16 respectively, Figure 12. Ligands 12, 15 and 17 displayed 3, 2, and 3 hydrogen bonds respectively. Other ligands (3, 5, 11 and 13) exhibited only one hydrogen bond. All ligands have a single hydrophobic bond with E166 except ligands 8 had 2. Another conserved residue among coronaviruses is F140 in P1, which has five hydrogen bonds and nine hydrophobic interactions. Each ligand of 12, 13, 14, 15 and 17 shows one of either hydrogen bond or hydrophobic interaction. Other ligands (3, 5 and 7) exhibit only one hydrophobic interaction. The rest of the residues in COVID-19 and other viruses such SARS-CoV interact with all 1,2,3-triazoles derivatives with at least one hydrophobic interaction, such as M165 (strongly alike among coronaviruses), and Q189 (weakly similar among coronaviruses). The total of interactions with M165 and Q189 are 16 and 14 respectively, Table S1.

An interesting comparative study, based on the binding affinity analyses, was conducted between the 1,2,3-triazole derivatives 3–17 of this research project and the US-FDA approved antiviral drugs with 6LU7 protease, Table 3.^[5,43] The binding affinities for the US-FDA approved antiviral drugs with 6LU7 protease were calculated especially for this study using PyRx, AutoDockVina, and the same parameter similar to those used for calculating the binding affinities for 1,2,3-triazole

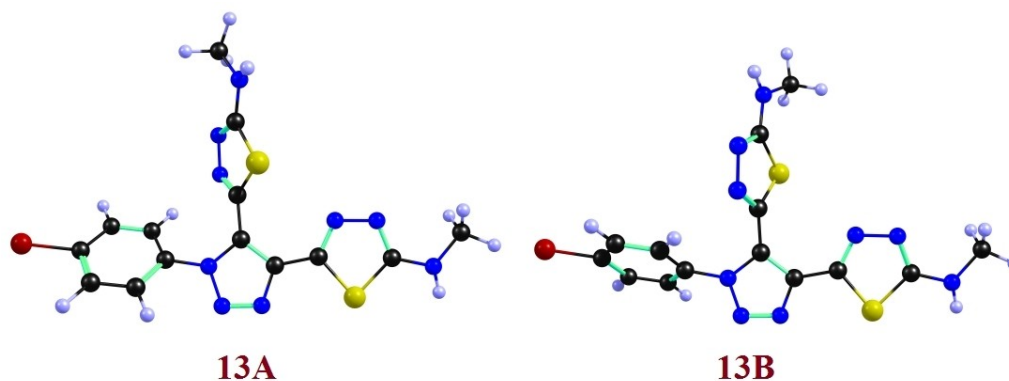


Figure 9. Optimized molecular structure of studied conformers A and B of bis-1,3,4-thiadiazole derivative 13.

Table 2. continued

Code^[a] Protease 6LU7 docked with 1,2,3-triazole derivatives properties

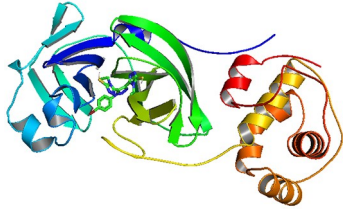
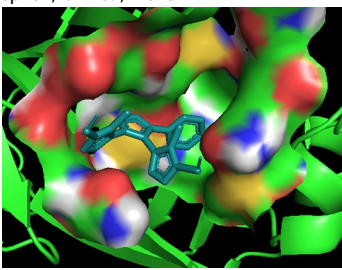
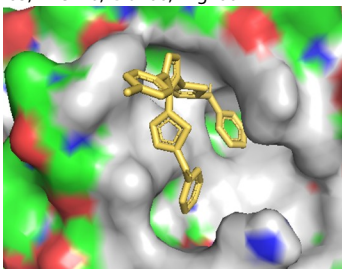
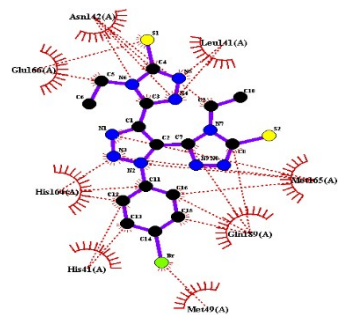
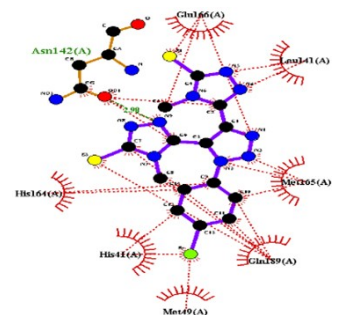
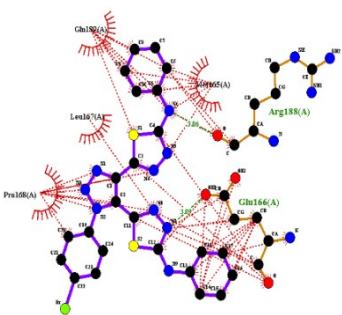
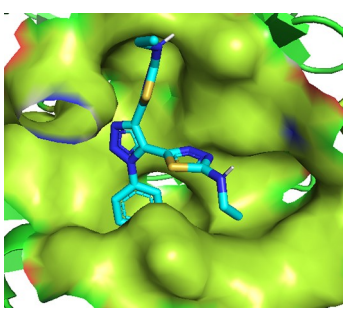
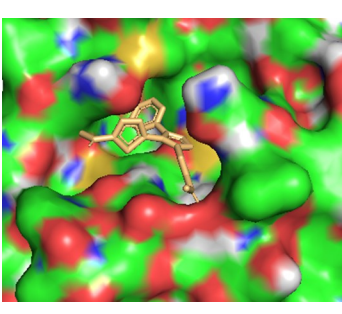
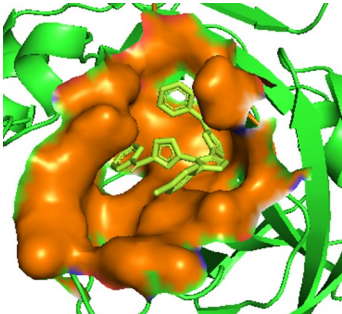
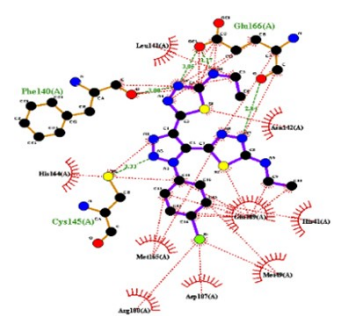
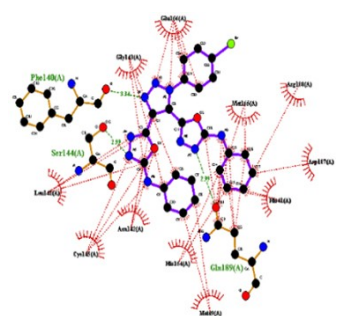
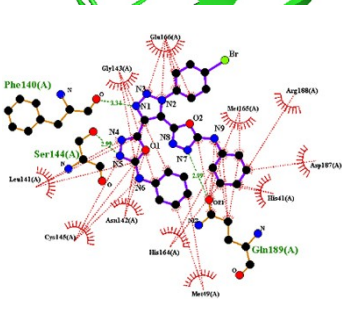
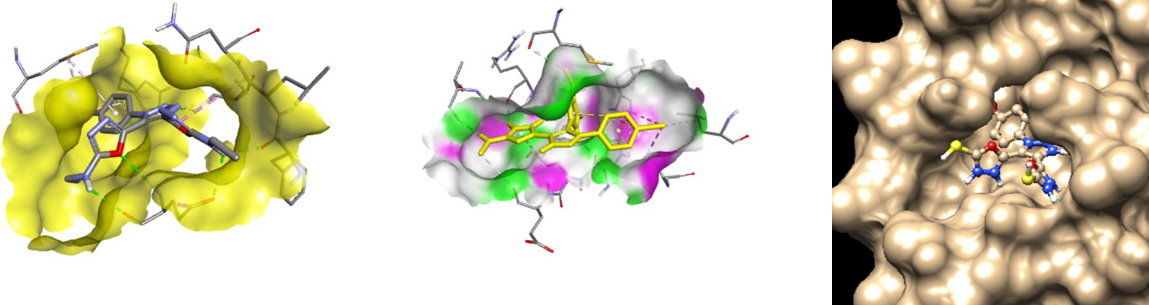
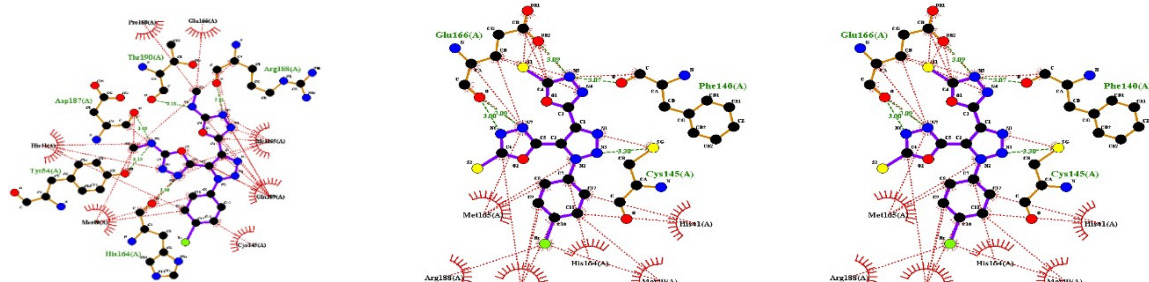
R4	5, His163(A), His41(A), His164(A), His164(A), Ser144 (A). 3.23, 3.26, 2.89, 3.09 and 3.14 Å respectively	4, His163(A), Asn142(A), Gly143(A), Gln189 (A), 2.80, 3.10, 2.89, 3.09 and 3.26 Å respectively	1, Gln189(A), 2.98 Å
R5	Met49, His164, Arg188, Met165, Asp187, Gln189, Glu166, Leu141, As142, Gly143, Thr26, Leu27, Ser144, Cys145, His163, His41	Thr25, Cys1455, Gly143, Phe140, Leu141, Asn142, His163, Arg188, Met165, Glu166, Asp187, Gln189, His164	Pro168, Gln192, Leu167, Thr190, Arg188, Glu166, Gln189, Met165, Asn142, Leu141, His165, Phe140, Glu166, Arg188
R1			
R2			
R3	9, -6.0, 0, 0, 0,	10, -6.3, 0, 0, 0,	11, -7.9, 0, 0, 0
R4	0	1, Asn142(A), 2.98 Å	2, Arg188(A), Glu166(A), 3.06, 3.09 and 3.09 Å respectively
R5	Met49, Gln189, His41, Met165, Leu141, Asl42, Glu166, His164	Met49, Gln189, Met165, Leu141, Glu166, Asn142, His41, His164	Gln189, Met165, Arg188, Leu167, Pro168, Glu166
R1			
R2			
R3	12, -7.0, 0, 0, 0	13, -7.2, 0, 0, 0	14, -8.8, 0, 0, 0
R4	5, Glu166(A), Glu166(A), Phe140(A), Cys145(A), Glu166(A), 2.84, 3.17, 3.00, 3.33 and 3.05 Å respectively	2, Glu166(A), Phe140(A), 2.97 and 2.90 Å respectively	3, Gln189(A), Ser144(A), Phe140(A), 2.99, 2.99 and 3.34 Å respectively
R5	Met165, Arg188, Asp187, Met49, His41, Asn142, Glu166, Leu141, Phe140, His164, Cys145, Gln189	Phe140, Asn142, Gln189, Met165, Met49, Asp187, His41, Arg188, His164, Cys145, Glu166	3, Gln189(A), Ser144(A), Phe140(A), 2.99, 2.99 and 3.34 Å respectively

Table 2. continued

Code^[a] Protease 6LU7 docked with 1,2,3-triazole derivatives properties

R1			
R2			
R3	15 , −7.4, 0, 0, 0	16 , −7.8, 0, 0, 0	17 , −7.1, 0, 0, 0
R4	3, Glu166(A), Glu166(A), Phe140(A), 3.00, 3.04 and 3.12 Å respectively	5, Thr190(A), Arg188 (A), Asp187(A), Tyr54 (A), His164(A), 3.21, 2.91, 3.05, 3.13 and 2.80 Å respectively	5, Glu166(A), Glu66(A), Glu66(A), Cys145(A), Phe140(A), 3.09, 3.09, 3.00, 3.30 and 3.07 Å respectively
R5	His164, His41, Met49, Cys145, Phe140, Asn142, Glu166, Met165, Gln189	Pro168, Glu166, Arg188, Thr190, Met165, Gln189, Cys145, His164, Met49, Tyr54, His41, Asp187	Phe140, Glu166, Met165, Arg188, Gln189, His164, Met49, His41, Cys145

[a]codes; (R1): 3D visualization of docking analysis of ligands protease binding with 6LU7; (R2): A Schematic 2-D LIGPLOT representation of 7BQY-triazole ligand complex; (R3): Compound number, binding affinities, mode, RMSD lower bond and RMSD upper bond; (R4): Number of H-bonds and the protein sites involved in the H-bonds; (R5): Hydrophobic residue bonds with the ligand. The purple bold lines, in the center, represent the ligand bonds, whereas the brown lines represent the active site (at the Gln189, Ser144 and Phe140 residues) involved in making hydrogen bonds with the ligand. The green dashed lines represent the hydrogen bonds whereas the red dashed thin lines and the spoked arcs pointing towards the ligand represent the hydrophobic residue bonds with the ligand. All atoms marked by spokes in the ligand or protein indicate which atoms are involved in the hydrogen and/or hydrophobic interactions.

Table 3. Docking data obtained in this study under the same conditions for known antiviral drugs and the 1,2,3-triazole derivatives 3–17, against 6LU7 for comparison.

Compound	Binding affinities kcal/mol	Compound	Binding affinities kcal/mol
1,2,3-triazole derivatives (3–17)	−6.0 to −8.8 ^[a]	Cloperastine	−7.0
Vigabatrin	−4.1	Ursolic acid	−7.1
Acetazolamide	−5.2	Nortriptyline	−7.3
Furidiazine (Triafur)	−6.1	Doravirine	−7.8
Desaglybuzole (Glybuzole)	−6.5	Methotrexate	−8.2
Hederagenin	−6.9	Maraviroc	−8.8
		Raltegravir	−9.6

[a] Details of binding affinities of 1,2,3-triazole derivatives of this study are presented in Table 2.

derivatives with 6LU7 protease. All the obtained docking results were achieved using the same conditions and parameters to ensure a fair comparison, Table 3. The binding affinities

detected for 1,2,3-triazole derivatives ranged from −6.0 to −8.8 kcal/mol. Figure 11 is demonstrating the effect of the functional groups of each compound on the binding affinity value. Whereas, the binding affinities for the antiviral drugs for Vigabatrin, Acetazolamide, Furidiazine (Triafur), Desaglybuzole (Glybuzole), Hederagenin, Cloperastine, Ursolic acid, Nortriptyline, Doravirine, Methotrexate, Maraviroc and Raltegravir are in the range of −4.1 to −9.6 kcal/mol, Table 3. Also, important known antiviral examples comparable to our results, in terms of docking scores using the same protease, 6LU7, which have been reported as potential COVID-19 medications: Remdesivir (−7.215 kcal/mol), Saquinavir (−7.285 kcal/mol), Indinavir (−8.199 kcal/mol) and Zanamivir (−8.843 kcal/mol).^[51] Also importantly, A–T. Ton and co-workers have identified recently the top 1,000 potential ligands for SARS-CoV-2 M^{pro} applying Deep Docking in conjunction with the Glide method to all 1.3 billion compounds obtained from Zinc-15 database.^[52,53] The 1000 virtual screened molecules, displayed binding affinities (docking scores) ranging from −11.32 to −9.00 kcal/mol which is comparable to our results.^[51] Based on these similar docking

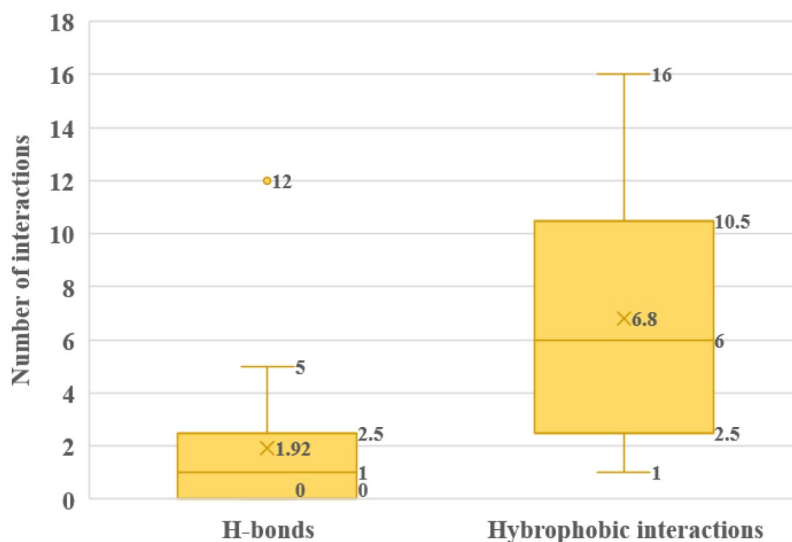


Figure 11. Box plot of number of H-bonds and hydrophobic interactions among amino acid residues of COVID-19 substrate binding sites and the 1,2,3-triazole derivatives.

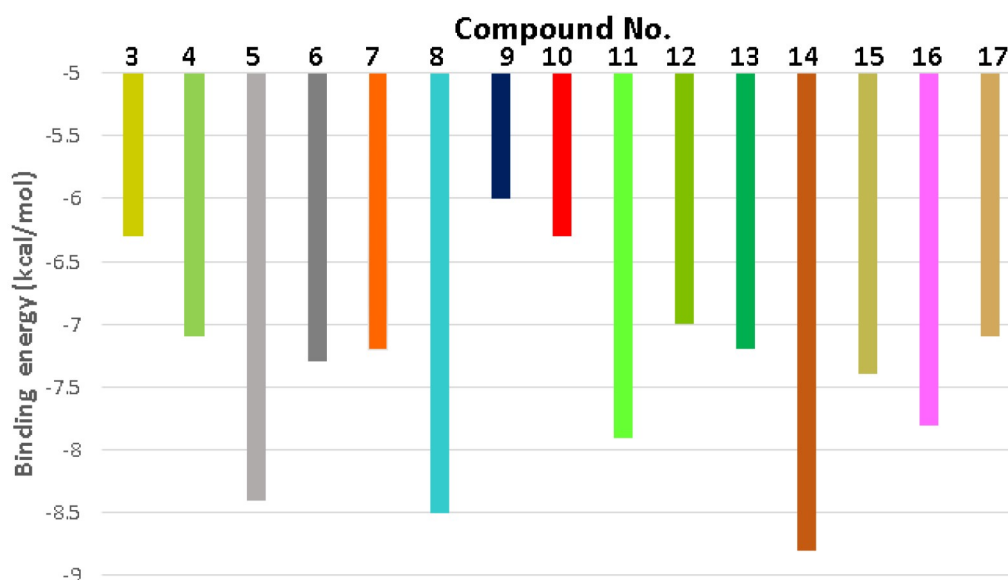


Figure 12. Binding affinities of 1,2,3-triazole derivatives 3–17 against COVID-19, 6LU7 protease.

The cut-off for the nonbonded interactions (neglecting hydrogen atoms) between the ligand and the amino acid residues, for the LIGPLOTs reported in this paper, is 3.9 \AA ,^[55] Figures 13 and 14.

Apparently, the total number of interactions (H-bonds and hydrophobic interactions) of each compound is directly related to the binding affinity value Table 2, Figure 11. In summary, the binding affinities of 1,2,3-triazole derivatives in this study: compounds 5, 8 and 14 are in the range of -8 to -8.8 . Compounds 4, 6, 7, 11, 12, 13, 15, 16 and 17 are in the range of -7.0 to 7.9 . Compounds 3, 9 and 10 are in the range of -6.0 to 6.9 kcal/mol, Figure 12.

Hydrophobic interactions and H-bonds between the substrate-binding pocket of COVID-19 (6LU7 protease) against the 1,2,3-triazole derivatives are summarized in Figure 14. These data are based on molecular docking study using PyRx, AutoDockVina, Table 2.

Further explanation about the interactions among amino acid residues of COVID-19 substrate binding sites and the 1,2,3-triazole derivatives, the M^{pro} alignment of coronaviruses was introduced in this study to authenticate the substrate-binding pocket of COVID-19 and other related viruses against the 1,2,3-triazole derivatives, Figure 15. This could throw light on the

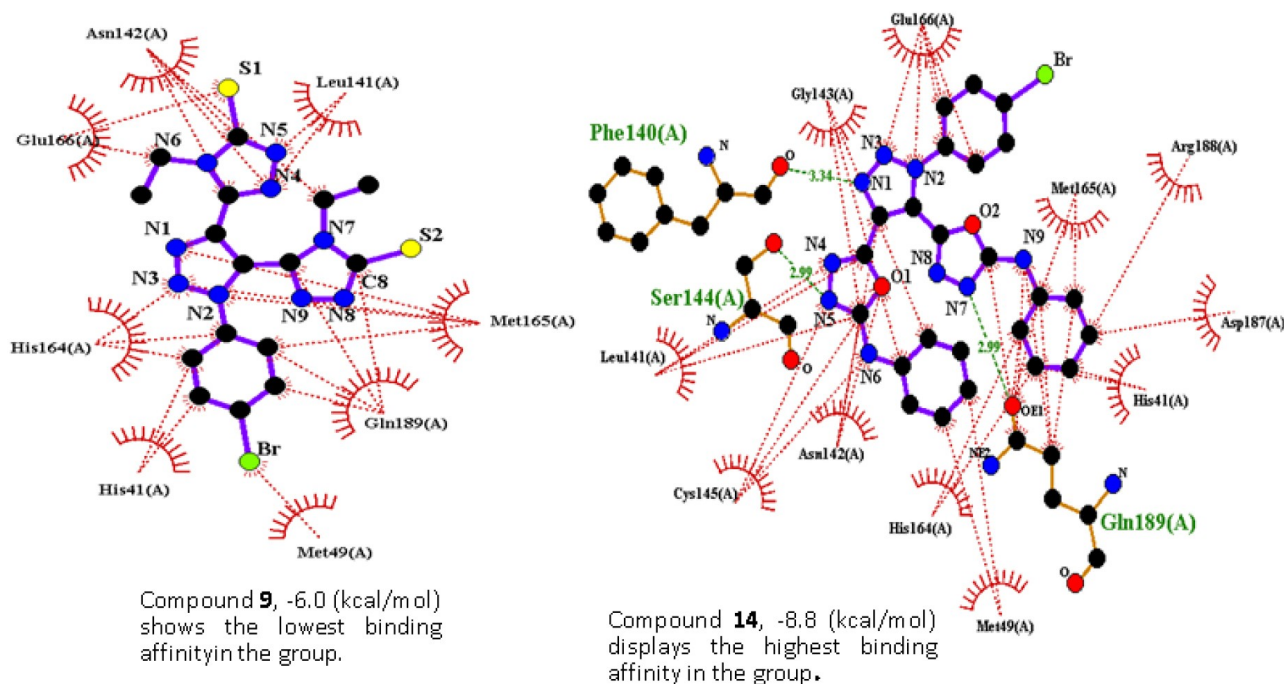


Figure 13. A schematic 2-D LIGPLOT representation of the SARS-CoV-2 main protease (M^{pro} , PDB code, 6LU7)-1,2,3-triazole ligand complex. A comparison between compounds **14** and **9** in terms of the number of interactions (H-bonding and hydrophobic) and binding affinity values. Compound **14** has the highest binding affinity whereas compound **9** has the least in the series. The purple bold lines, in the center, represent the ligand bonds, whereas the brown lines represent the active site (at the Gln189, Ser144 and Phe140 residues) involved in making hydrogen bonds with the ligand. The green dashed lines represent the hydrogen bonds whereas the red dashed thin lines and the spoked arcs pointing towards the ligand represent the hydrophobic residue bonds with the ligand. All atoms marked by spokes in the ligand or protein indicate which atoms are involved in the hydrogen and/or hydrophobic interactions.

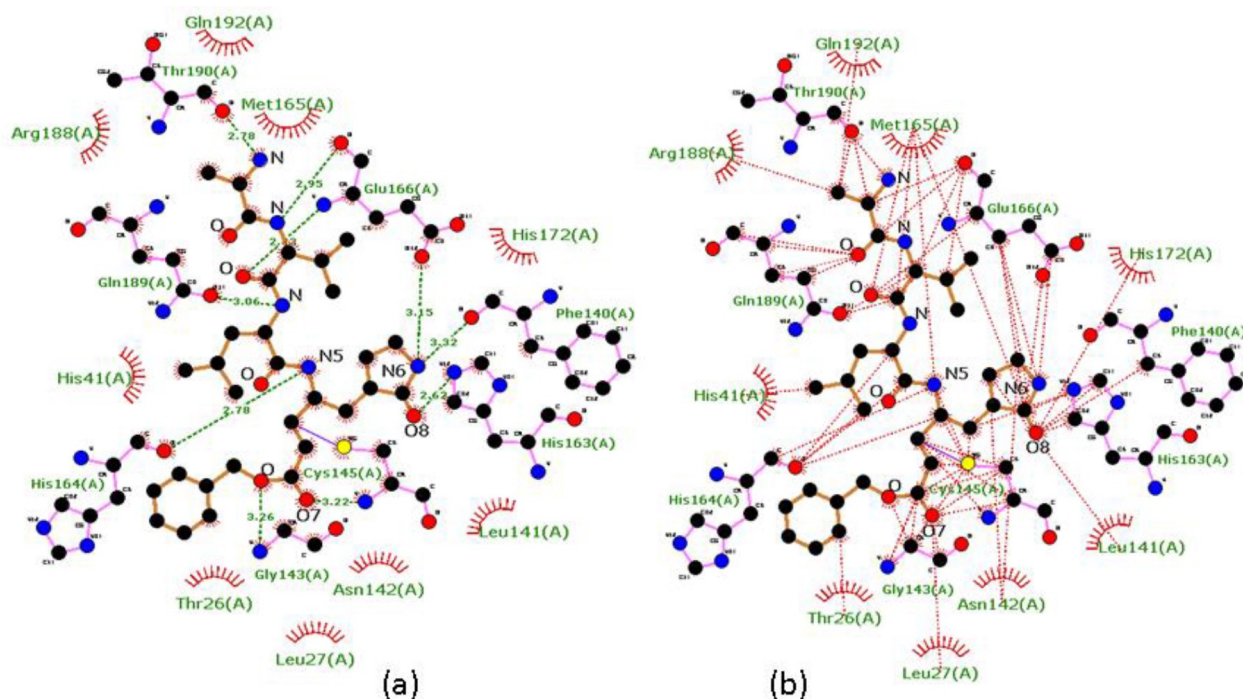


Figure 14. Schematic 2-D LIGPLOTs, calculated especially in this study for the inhibitor **N3** and the SARS-CoV-2 main protease for comparison with the newly synthesized 1,2,3-triazole derivatives of this study.^[43] A key to the symbols is shown in Figure 8. (a) only H-bonds interactions are shown; (b) only hydrophobic interactions are shown.

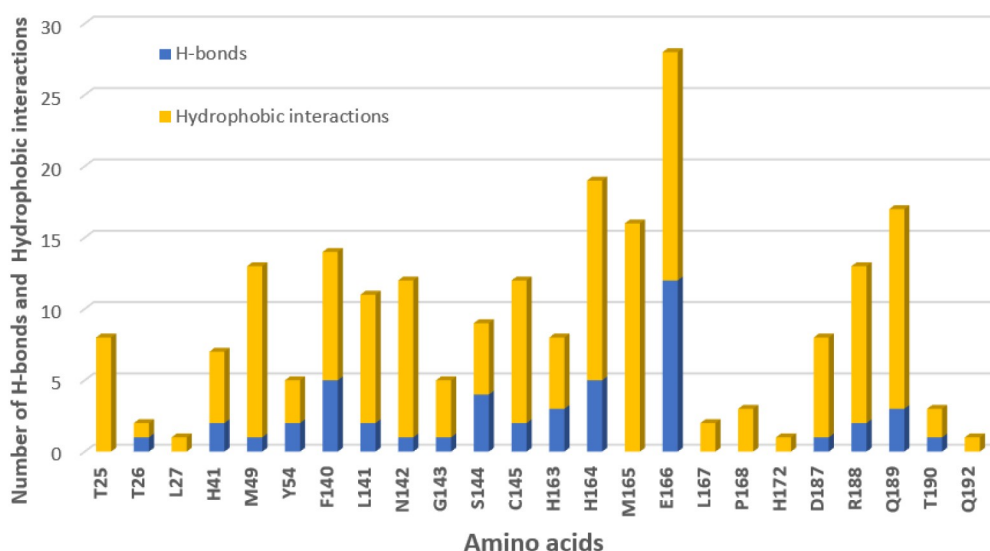


Figure 15. Number of hydrophobic interactions and H-bonds between 6LU7 protease against the 1,2,3-triazole derivatives based on the docking data in Table 2.

1,2,3-triazole derivative(s) as a wide range of anti-coronavirus drugs.

3. Conclusion

A novel series of 1,2,3-triazoles based-1,2,4-triazole, 1,3,4-oxadiazole and/or 1,3,4-thiadiazole skeletons were modeled and efficiently synthesized. The spectroscopic data of the synthesized compounds illustrated the presence of an isomeric mixture between two proposed conformers and these data were confirmed by the DFT simulation to show that the stability of one isomeric form with respect to the other in the range of 0.057–0.161 Kcal mol⁻¹. However, the ratios of projected conformers were found to be affected by the size of the attached group as well as the type of the heteroatom forming the side ring. Based on the observations of virtual screening established using molecular docking performed to identify novel compounds that can be able to bind with protein structures of COVID-19 (PDB ID: 6LU7), we believed that the 1,2,3-triazole derivatives could aid in COVID-19 drug discovery. This is clearly manifested in the bond affinity obtained for ligands 3–17 indicating good binding potency against COVID-19. Authentication of the docking results was performed using the M^{pro} alignment of coronavirus substrate-binding pockets of COVID-19 against the 1,2,3-triazole derivative. In the future, these ligands could be used for the initiation of clinical trials.

Supporting information

The detailed experimental data including organic synthesis methodologies, characterization, molecular docking and computational methods and calculations are all reported in supporting information.

Acknowledgment

Musa A. Said is thankful to AvH for the continuous support.

Conflict of Interest

The authors declare no conflict of interest.

Keywords: Covid-19 · DFT conformational study · Main Protease molecular docking · 1,2,3-Triazole

- [1] K. A. Peele, C. Potla Durthi, T. Srihansa, S. Krupanidhi, A. V. Sai, D. J. Babu, M. Indira, A. R. Reddy, T. C. Venkateswarulu, *Informatics Med. Unlocked* **2020**, *19*, 100345–100350.
- [2] D. S. V. Shah, J. Bhaliya, *ChemRxiv*, **2020**, *19*, 1–15.
- [3] B. Shah, P. Modi, S. R. Sagar, *Life Sci.* **2020**, *252*, 117652–117664.
- [4] R. Yu, L. Chen, R. Lan, R. Shen, P. Li, *Int. J. Antimicrob. Agents* **2020**, *2*, 106012–106024.
- [5] N. Chauhan, *ChemRxiv*, **2020**, 1–4.
- [6] C. J. Cortés-García, L. Chacón-García, J. E. Mejía-Benavides, E. Díaz-Cervantes, *PeerJ* **2020**, *2*, 1–26.
- [7] C. Wang, P. W. Horby, F. G. Hayden, G. F. Gao, *A novel coronavirus outbreak of global health concern*, Vol. 395, Lancet Publishing Group, **2020**, pp. 470–473.
- [8] L. Zou, F. Ruan, M. Huang, L. Liang, H. Huang, Z. Hong, J. Yu, M. Kang, Y. Song, J. Xia, Q. Guo, T. Song, J. He, H. L. Yen, M. Peiris, J. Wu, *SARS-CoV-2 viral load in upper respiratory specimens of infected patients*, Vol. 382, Massachusetts Medical Society, **2020**, pp. 1177–1179.
- [9] T. Singhal, *A Review of Coronavirus Disease-2019 (COVID-19)*, Vol. 87, Springer, **2020**, pp. 281–286.
- [10] D. Wang, B. Hu, C. Hu, F. Zhu, X. Liu, J. Zhang, B. Wang, H. Xiang, Z. Cheng, Y. Xiong, Y. Zhao, Y. Li, X. Wang, Z. Peng, *JAMA J. Am. Med. Assoc.* **2020**, *323*, 1061–1069.
- [11] L. Zhang, Y. Liu, *Potential interventions for novel coronavirus in China: A systematic review*, Vol. 92, John Wiley and Sons Inc., **2020**, pp. 479–490.
- [12] Z. M. Chen, J. F. Fu, Q. Shu, Y. H. Chen, C. Z. Hua, F. B. Li, R. Lin, L. F. Tang, T. L. Wang, W. Wang, Y. S. Wang, W. Z. Xu, Z. H. Yang, S. Ye, T. M. Yuan, C. M. Zhang, Y. Y. Zhang, *Diagnosis and treatment recommendations for pediatric respiratory infection caused by the 2019 novel*

- coronavirus, Vol. 16, Institute of Pediatrics of Zhejiang University, 2020, pp. 240–246.
- [13] K. Karypidou, S. R. Ribone, M. A. Quevedo, L. Persoons, C. Pannecouque, C. Helsen, F. Claessens, W. Dehaen, *Bioorg. Med. Chem. Lett.* **2018**, *28*, 3472–3476.
- [14] M. H. Sampangi-Ramaiah, R. Vishwakarma, R. U. Shaanker, *Curr. Sci.* **2020**, *118*, 1087–1092.
- [15] S. Asadi, N. Bouvier, A. S. Wexler, W. D. Ristenpart, *Aerosol Sci. Technol.* **2020**, *54*, 635–638.
- [16] K. Dhama, K. Sharun, R. Tiwari, M. Dadar, Y. S. Malik, K. P. Singh, W. Chaicumpa, *Hum. Vaccines* **2020**, *16*, 1232–1238.
- [17] K.-C. Chou, *Front. Med. Chem.* **2012**, 455–502.
- [18] I. D. Kuntz, J. M. Blaney, S. J. Oatley, R. Langridge, T. E. Ferrin, *J. Mol. Biol.* **1982**, *161*, 169–288.
- [19] R. W. Sidwell, J. H. Huffman, G. P. Khare, L. B. Allen, J. T. Witkowski, R. K. Robins, *Science* **1972**, *177*, 705–706.
- [20] A. Krajczyk, K. Kulinska, T. Kulinski, B. L. Hurst, C. W. Day, D. F. Smees, T. Ostrowski, P. Januszczyk, J. Zeidler, *Antiviral Chem. Chemother.* **2014**, *23*, 161–171.
- [21] S. M. Cohen, E. Erturk, A. M. von Esch, A. Corvetto, G. Bryan, *J. Natl. Cancer Inst.* **1975**, *54*, 841–850.
- [22] Y. Bashir, M. Kann, J. R. Stradling, *Pulm. Pharmacol.* **1990**, *3*, 151–154.
- [23] F. K. Guirgis, M. H. Ghanem, M. M. Abdel Hay, *Arzneimittel-Forschung/Drug Res.* **1976**, *26*, 435–437.
- [24] N. Rezki, *Molecules* **2016**, *21*, 505–518.
- [25] Y. Zhu, H. Li, K. Lin, B. Wang, W. Zhou, *Synth. Commun.* **2019**, *49*, 1721–1728.
- [26] S. G. Khalilieh, K. L. Yee, R. I. Sanchez, L. Fan, M. S. Anderson, M. Sura, T. Laethem, S. Rasmussen, L. Van Bortel, G. van Lancker, M. Iwamoto, *Antimicrob. Agents Chemother.* **2019**, *63*, 1–14.
- [27] K. Bozorov, J. Zhao, H. A. Aisa, *Bioorg. Med. Chem.* **2019**, *27*, 3511–3531.
- [28] R. Ramesh, A. Lalitha, *ChemistrySelect* **2016**, *1*, 2085–2089.
- [29] N. Ivanović, L. Jovanović, Z. Marković, V. Marković, M. D. Joković, D. Milenković, P. T. Djurdjević, A. Ćirić, L. Joksović, *ChemistrySelect* **2016**, *1*, 3870–3878.
- [30] P. A. Channar, A. Saeed, F. A. Larik, M. Bolte, M. F. Erben, *J. Mol. Struct.* **2019**, *1179*, 11–17.
- [31] A. Saeed, Z. Ashraf, H. Nadeem, J. Simpson, H. Pérez, M. F. Erben, *J. Mol. Struct.* **2019**, *1195*, 796–806.
- [32] A. Allouche, *J. Comput. Chem.* **2012**, *32*, 174–182.
- [33] J. H. Boyer, F. C. Canter, *Chem. Rev.* **1954**, *54*, 1–57.
- [34] I. B. Douglass, F. B. Dains, *J. Am. Chem. Soc.* **1934**, *56*, 719–721.
- [35] A. Saeed, M. N. Mustafa, M. Zain-ul-Abideen, G. Shabir, M. F. Erben, U. Flörke, *J. Sulfur Chem.* **2019**, *40*, 312–350.
- [36] E. S. H. El Ashry, L. F. Awad, S. M. Soliman, M. N. Abd Al Moaty, H. A. Ghabbour, A. Barakat, *J. Mol. Struct.* **2017**, *1146*, 432–440.
- [37] M. R. Aouad, N. Rezki, M. A. Said, D. Lentz, L. Zubaydi, I. Warad, *J. Mol. Struct.* **2019**, *1180*, 455–461.
- [38] M. R. Aouad, M. Messali, N. Rezki, N. Al-Zaqri, I. Warad, *J. Mol. Liq.* **2018**, *264*, 621–630.
- [39] P. A. Channar, A. Saeed, M. F. Erben, F. A. Larik, S. Riaz, U. Flörke, M. Arshad, *J. Mol. Struct.* **2019**, *1191*, 152–157.
- [40] Naveen, R. K. Tittal, V. D. Ghule, N. Kumar, L. Kumar, K. Lal, A. Kumar, *J. Mol. Struct.* **2020**, *1209*, 127951.
- [41] S. L. Laurella, M. F. Erben, *Spectrochim. Acta Part A* **2016**, *164*, 40–42.
- [42] D. X. Liu, J. Q. Liang, T. S. Fung, *Ref. Modul. Life Sci., Elsevier*, **2020**, 428–440.
- [43] Z. Jin, X. Du, Y. Xu, Y. Deng, M. Liu, Y. Zhao, B. Zhang, X. Li, L. Zhang, C. Peng, Y. Duan, J. Yu, L. Wang, K. Yang, F. Liu, R. Jiang, X. Yang, T. You, X. Liu, X. Yang, F. Bai, H. Liu, X. Liu, L. W. Guddat, W. Xu, G. Xiao, C. Qin, Z. Shi, H. Jiang, Z. Rao, H. Yang, *Nature* **2020**, *582*, 289–293.
- [44] Y. Liming, C. Yang, Z. Rao, Z. Ren, L. Yan, N. Zhang, Y. Guo, C. Yang, Z. Lou, Z. Rao, *Protein Cell* **2013**, *4*, 248–250.
- [45] F. Wang, C. Chen, W. Tan, K. Yang, H. Yang, *Sci. Rep.* **2016**, *6*, 22677.
- [46] X. Xue, H. Yu, H. Yang, F. Xue, Z. Wu, W. Shen, J. Li, Z. Zhou, Y. Ding, Q. Zhao, X. C. Zhang, M. Liao, M. Bartlam, Z. Rao, *J. Virol.* **2008**, *82*, 2515–2527.
- [47] H. Yang, M. Yang, Y. Ding, Y. Liu, Z. Lou, Z. Zhou, L. Sun, L. Mo, S. Ye, H. Pang, G. F. Gao, K. Anand, M. Bartlam, R. Hilgenfeld, Z. Rao, *Proc. Natl. Acad. Sci.* **2003**, *100*, 13190–13195.
- [48] K. Anand, G. J. Palm, J. R. Mesters, S. G. Siddell, J. Ziebuhr, R. Hilgenfeld, *EMBO J.* **2002**, *21*, 3213–3224.
- [49] F. Sievers, D. G. Higgins, *Protein Sci.* **2018**, *27*, 135–145.
- [50] F. Sievers, A. Wilm, D. Dineen, T. J. Gibson, K. Karplus, W. Li, R. Lopez, H. McWilliam, M. Remmert, J. Söding, J. D. Thompson, D. G. Higgins, *Mol. Syst. Biol.* **2011**, *7*, 1–6.
- [51] D. C. Hall, H. F. Ji, *Travel Med. Infect. Dis.* **2020**, *35*, 101646.
- [52] A. T. Ton, F. Gentile, M. Hsing, F. Ban, A. Cherkasov, T. Sterling, J. J. Irwin, *Mol. Inf.* **2020**, *39*, 1–8.
- [53] T. Sterling, J. J. Irwin, *J. Chem. Inf. Model.* **2015**, *55*, 2324–2337.
- [54] D. A. Sabbah, F. Al-Tarawneh, W. H. Talib, K. Sweidan, S. K. Bardaweel, E. Al-Shalabi, H. A. Zhong, G. Abu Sheikha, R. Abu Khalaf, M. S. Mubarak, *Med. Chem.* **2018**, *14*, 695–708.
- [55] A. C. Wallace, R. A. Laskowski, J. M. Thornton, *Protein Eng. Des. Sel.* **1995**, *8*, 127–134.

Submitted: February 16, 2021

Accepted: March 25, 2021